

Two-Dimensional DoA Estimation for Multipath Propagation Characterization Using the Array Response of PN-Sequences

Ruonan Zhang, *Member, IEEE*, Shichao Wang, *Student Member, IEEE*, Xiaofeng Lu, Weiming Duan, and Lin Cai, *Senior Member, IEEE*

Abstract—Multipath propagation and power arrival profiles in three-dimensional (3-D) space determine the performance of the full-dimensional MIMO (FD-MIMO) systems. Field channel measurements are crucial in characterizing wireless channel properties. Nevertheless, in spatial channel measurements, estimating the direction-of-arrivals (DoAs) of multipath components (MPCs) is a challenging issue, because of the large number of propagation paths and the correlation among the multipath signals. The number of incidence angles and estimation precision in traditional methods is limited by the sensor array size and signal correlation. In this paper, we propose a scheme for measuring and estimating the 2-D DoAs of propagation paths called multipath angular estimation using the array response of PN-sequences (MAPS). By using a receiving planar antenna array (PAA), MAPS first extracts the complex path array response vector (PARV) for each propagation path and then estimates the DoAs of the paths individually and independently. The subspace-decomposition theory for MAPS is proved and extensive simulations are conducted to compare MAPS with other algorithms. Furthermore, a channel sounder using two PAAs and the probing signal of 2.6 GHz carrier modulated by PN-sequences has been developed. The simulation and field tests show that MAPS can estimate arbitrary number of resolved MPCs in a channel snapshot and effectively suppress the multipath interference.

Index Terms—Channel measurement, DoA estimation, multipath propagation, channel sounder.

I. INTRODUCTION

PLANAR antenna arrays will be employed at base stations in the next-generation cellular networks to realize the full-dimensional multiple-input-multiple-output (FD-MIMO) communications [1]. By using beamforming and sectorization in both the azimuth and elevation domains, the network capacity can be improved substantially. The potential of FD-MIMO

Manuscript received December 5, 2014; revised May 12, 2015; accepted August 12, 2015. Date of publication August 26, 2015; date of current version January 7, 2016. The associate editor coordinating the review of this paper and approving it for publication was Dr. Christopher R Anderson.

R. Zhang and S. Wang are with the Department of Communications Engineering and the Internet-of-Things Technologies and Applications Laboratory, Northwestern Polytechnical University, Xi'an 710072, China (e-mail: rzhang@nwpu.edu.cn; wangshichao@mail.nwpu.edu.cn).

X. Lu and W. Duan are with the Huawei Technologies Ltd., Shanghai 201206, China (e-mail: Stan.Lu@huawei.com; weiming.duan@huawei.com).

L. Cai is with the Department of Electrical and Computer Engineering, University of Victoria, Victoria, BC V8W 3P6, Canada (e-mail: cai@ece.uvic.ca).

Color versions of one or more of the figures in this paper are available online at <http://ieeexplore.ieee.org>.

Digital Object Identifier 10.1109/TWC.2015.2473156

depends on both the design of active antennas and the spatial characteristics of the cellular radio channels [2]. Therefore, measurement and modeling of multipath propagations in three-dimensional (3D) space have attracted great attention recently. In 2012, 3GPP initialized a study item (SI) [3] and called for proposals for 3D MIMO channel models describing the *azimuth/elevation angle-of-arrival (AoA/EoA)* of each propagation path and the large-scale spatial fading parameters, such as the *root-mean-square (rms) azimuth/elevation spread of arrival (ASA/ESA)*.

To validate the stochastic channel models and assist parameter selection, extensive field measurements of the two-dimensional direction-of-arrival (2D DoA), *i.e.*, AoA and EoA, of multipath components (MPCs) in radio channels are necessary. Accurate and efficient 2D DoA estimation methods for propagation paths is critical in multipath channel measurement and modeling. Nevertheless, the received sounding signals in channel probing have two features: 1) the presence of a large number of impinging waves (*i.e.*, MPCs) with different DoAs and 2) the high correlation among them. These facts pose great challenges in estimating the DoAs of multipath propagations.

One method to measure the spatio-temporal characteristics of radio channels is using a precise positioning system to move and rotate a directional receiver antenna on a linear track [4]. However, this approach requires a sophisticated mechanical structure and complicated operations during field measurements. Using a planar antenna array (PAA) and estimating the DoAs of MPCs based on the captured array signals is an alternative way to measure spatial channels. With this approach, the PAA can be fixed and the physical movement or rotation of antennas is not needed.

The traditional DoA estimation algorithms, such as maximum likelihood (ML) [5], MUSIC [6], ESPRIT [7], Matrix Pencil (MP) [8], and their variants [9]–[12], have been designed for emitter positioning. The MUSIC algorithm uses the orthogonality between the antenna array's steering vectors and the noise subspace to generate the spatial spectra of received array signals. The peaks of a spectrum indicate the directions of signal sources. The 2D MUSIC extends the spectra into two-dimensions, while the operations remain the same [13]. The UCA-ESPRIT [14] and Unitary-ESPRIT algorithms [15] have been proposed to use a uniform circular array and a rectangular array, respectively. The former is based on the signal subspace invariance resulting from the centro-symmetric

structure of the sensor array, while the latter decreases the computational complexity by transforming the complex array directional matrix and signal covariance matrix into real matrices. Proposed by Marcos *et al.* [16], the propagator method (PM) opens up a new direction for 2D DoA estimation, and has been followed by many works such as [17] and [18]. PM is a subspace-based method but does not require the eigen-decomposition of the received signals' covariance matrix, so it consumes much less computational resources.

DoA estimation is still an active research topic in recent years. The above approaches have been extended with coherent sources [19], [20]. The method in [19] reconstructs a special data matrix from the range-compressed received data and the average of multiple pulses is used to obtain the signal and noise subspaces. The singular value decomposition (SVD) based ESPRIT algorithm is then used to find the DoAs. This method requires a symmetrical array mode on both the transmitter and receiver sides. In [20], the authors proposed a modified PM for estimating the 2D DoAs of multiple coherently distributed sources, using three parallel uniform linear arrays. In [21], a fast search-free method using coprime arrays was proposed. The method estimates DoAs by each uniform linear subarray separately and then combines the results with a projection method, which substantially reduces the complexity. The method in [22] was designed for the case where a number of uncorrelated and coherent narrow-band signals existed simultaneously. It first estimates uncorrelated sources via conventional subspace methods and then eliminates them by spatial differentiation. Finally the remaining coherent signals are estimated using the spatial differentiating matrix. In [23], a computationally efficient subspace algorithm was developed for 2D DoA estimation using an L-shaped array. The algorithm obtains the noise subspace by rearranging the elements of the correlation matrix. The authors in [24] present a closed-form algorithm for estimating the 3 D location including the AoA, EoA, and range of a single source by using a uniform circular array.

Although the above methods have provided useful tools for emitter/source localization, they have a common requirement that the number of impinging waves (*i.e.*, DoAs to estimate) should be smaller than the number of array sensors. In addition, they were designed originally for uncorrelated source signals. Although some of the approaches have been extended to operate with correlated sources, their performance in terms of precision and signal-to-noise ratio (SNR) tolerance is sacrificed and the algorithm complexity increases considerably. The multipath DoA estimation issue in spatial channel measurement is essentially different from the traditional emitter localization problem and more challenging because of the large number of impinging waves and the high correlations among them. Therefore, traditional approaches for DoA estimation may not be applicable to this application.

For the purpose of channel modeling, the ML method, called space-alternating generalized expectation-maximization (SAGE) [25], [26], has been widely applied to extract path parameters from channel measurement data. By performing iterative joint expectation-maximization (EM) on several parameters (such as relative delay, incidence angle, Doppler frequency, and complex amplitude) of the impinging waves,

SAGE can separate waves and obtain multiple parameter estimations by searching in different domains simultaneously. Nevertheless, EM searching iterations on several parameters results in a very high computational complexity. Although the ML method (such as SAGE) is suitable for the DoA estimation in channel measurements, the subspace-decomposition approaches (like MUSIC and ESPRIT) require much less computational time and resources, which is vital for massive channel measurement campaigns.

Motivated by the need for efficient multipath 2D DoA estimation in massive channel measurements, we propose a new scheme, called *Multipath angular estimation based on the Array response of PN-Sequences (MAPS)*, which is designed to estimate the AoA and EoA of MPCs using a PAA. The main contributions of this paper are three-fold.

First, the MAPS scheme is proposed and the underlying subspace-decomposition theory is proved analytically. When measuring a radio channel at a given frequency band, the carrier is modulated by pseudo-noise (PN) sequences and transmitted to probe wireless channels. The propagation paths are first identified by the time-domain channel response of the PN-sequences based on their auto-correlation property. Since the complex channel response on the antenna array contains the carrier phase shift information, the *path array response vector (PARV)* for each resolved path is constructed. Then, based on the subspace-decomposition theory, the 2D spatial spectrum for each MPC is calculated and its AoA and EoA are jointly estimated by single peak searching. In addition, for dense multipath environments where multiple paths may arrive within one chip duration of the PN-sequences, two methods have also been proposed in this paper. One is by over-sampling of the received waveforms and successive path deduction to resolve the paths in time-domain with much higher resolution. The second method is the spatial smoothing on received PARVs which can resolve the paths within one chip duration in space-domain.

Second, extensive simulations are conducted to compare the performance (in terms of estimation error and angular resolution) of MAPS with other methods including MUSIC, CAPON, ESPRIT, MP, and, SAGE with various array sizes, propagation path numbers and SNR. The simulation results illustrate that, because MAPS estimates the DoA of each propagation path separately and suppresses the multipath interference, it can estimate the DoAs of more paths with a higher resolution given the same SNR and array size.

Third, a channel sounder equipped with two 4×4 PAAs has been developed and field measurements in two scenarios were conducted to test the proposed MAPS scheme. By implementing a direct-sequence spread spectrum (DSSS) transmission system, the sounder probes a radio channel by a 2.6 GHz carrier that is modulated by the repeat of a 1,023-bit PN-sequence. In one test scenario, the line-of-sight (LOS) path between the transceivers with a controlled incidence angle was measured, while in the other scenario the multipath propagations in a typical LOS street canyon environment were measured. The results showed that the estimated 2D DoAs had a good match with the expected spatial propagations according to the scattering environment. The field tests validate the application of MAPS for practical channel measurements.

MAPS has several salient features. 1) Differing from traditional methods that directly use the received radio frequency (RF) signals, MAPS first distinguishes the propagation paths based on the channel response on PN-sequences and then estimates their DoAs separately. Due to the peak shape of the auto-correlation function of the PN-sequences, the superimposed signals through different paths can be distinguished. In dense multipath environments (like indoor channels), the paths arriving at the receiver within one chip duration can be resolved by successive deduction and spatial smoothing jointly in time-space-domain. Even if two paths arrive at the receiver at the same time, they cannot be resolved in the time-domain, but can be separated in the space-domain and estimated for DoAs. On the other hand, if two paths arrive at the same incidence angle, they can be separated first in the time-domain and then their DoA is estimated. Thus, the proposed scheme can estimate a large number of paths, which is not limited by the antenna array size. 2) Since each MPC is processed individually based on its PARV rather than the original received signals, the correlation among the multipath signals is removed and does not affect the performance. 3) In traditional methods such as MUSIC and CAPON, an obtained spatial spectrum has multiple peaks for all the emitters' DoAs. Consequently, the angular resolution is twice that of the antenna pattern (the minimum angular interval between the steering vectors). In MAPS, however, if two paths are distinguished in the time-domain PN-sequence response, their incident angles can be estimated even if the angles are the same. Therefore, MAPS uses the high temporal resolution to achieve a high spatial resolution. 4) In the DoA estimation of one path, the interferences from the other paths can be effectively suppressed by using the PN-sequence correlation operation. The spread spectrum gain leads to significantly increased signal-to-interference-ratio (SIR) and accuracy of DoA estimation. 5) The PAA in MAPS can be of an arbitrary shape, like a square, rectangular, circular or "L" shape, and the centro-symmetric structure is not required. Thanks to the low hardware requirement and computational complexity, MAPS is easy to implement in practical channel sounder systems.

MAPS can also be used for cooperative node localization in wireless networks. For example, some anchor nodes can broadcast PN-sequence modulated carriers over the air. When a node equipped with an antenna array receives the signals from at least two anchors, it can estimate their directions using the proposed MAPS scheme and then determine its own location. The advantage of MAPS is that it can not only estimate the DoAs of the anchors' signals but also suppress their mutual interference. Furthermore, if more anchors exist, the node can estimate all of their directions to increase the localization precision, without the need to increase the antenna array size (even using only two antenna elements in one dimension).

The rest of the paper is organized as follows. In Sec. II, the multipath wireless channel model is presented and the 2D-DoA estimation algorithm of MAPS is proved theoretically. Two path extraction methods, the time-domain over-sampling and successive deduction and the space-domain spatial smoothing, are proposed in Sec. III for DoA estimation in dense multipath environments. The algorithm implementation is given in Sec. IV. Sec. V presents the simulation results to compare the

performance of MAPS and several traditional algorithms. The implementation of the channel sounder based on the MAPS scheme and the field experiments are presented in Sec. VI. Sec. VII concludes the paper and points out future research issues.

II. SUBSPACE-DECOMPOSITION THEORY OF MAPS

A. Spatial Channel Impulse Response Model

With the objective of characterizing the spatial propagation in radio channels, we adopt a 3 D channel model which incorporates the time-of-arrival (ToA) and 2D DoA (including AoA and EoA in azimuth and elevation dimensions, respectively) information. In a static multipath channel, the channel impulse response (CIR) is time-invariant and expressed as

$$h(\tau) = \sum_{l=1}^L h_l^{CH} e^{j\eta(\phi_l, \theta_l)} \delta(\tau - \tau_l), \quad (1)$$

where L is the number of resolvable paths, h_l^{CH} , τ_l , ϕ_l , and θ_l are the complex gain, excess delay, AoA, and EoA of the l -th path, respectively. $\eta(\phi_l, \theta_l)$ is the phase shift with respect to the reference point and is related to the incidence angle. The DoA in (1) is defined with respect to the X - Y - Z coordinate system illustrated in Fig. 13(d).

B. Time-domain Channel Response on PN-sequence

The time-domain channel sounding uses a carrier modulated by PN-sequences to probe wireless channels, and the multipath channel responses are captured by a PAA. A PN-sequence with the length of K bits (chips), denoted by $a(t)$, is expressed as

$$a(t) = \sum_{k=0}^{K-1} b_k \mathbf{rect}_{T_b}(t - kT_b), \text{ for } b_k \in \{+1, -1\} \quad (2)$$

where $\mathbf{rect}_{T_b}(t)$ denotes a rectangular pulse with the duration of one bit T_b and the power of $P_b = \int_0^{T_b} \mathbf{rect}_{T_b}^2(\tau) d\tau$. The duration of the PN-sequence is $T_p = KT_b$. Several PN-sequences are concatenated to form a frame and, in each frame, a cyclic prefix and postfix can be added as the safe guard periods for antenna switching and signal capture. The frames are modulated on a carrier and transmitted over the air.

The antenna array of the receiver (Rx) consists of M elements which are placed on a plane. In practical channel measurements, the Rx is usually far away from the transmitter (Tx) such that the impinging waves at the Rx array can be regarded as specular plane waves. In addition, the probing signals are assumed to be narrow-band, *i.e.*, $B_s \ll f_c$ where B_s and f_c are the signal bandwidth and carrier frequency, respectively.

Suppose that there are L multipath waves impinging at the Rx, so that the output signal of the m -th element for the duration of one PN-sequence, T_p , in the delay domain is

$$\tilde{y}_m(\tau) = \sum_{l=1}^L h_l^{CH} s_m(\phi_l, \theta_l) a(\tau - \tau_l) + N_m(\tau), \quad (3)$$

where $s_m(\phi_l, \theta_l)$ is the *complex steering factor* of the m -th element at the incidence angle of (ϕ_l, θ_l) and $N_m(\tau)$ is the Gaussian noise process. In (3), $a(\tau - \tau_l)$ is the circular shift of $a(\tau)$ by the delay of τ_l .

The steering vector $s_m(\phi, \theta)$ can be decomposed as

$$s_m(\phi, \theta) \triangleq g_m(\phi, \theta)e^{[j\psi_m + j\eta_m(\phi, \theta)]} = g_m(\phi, \theta)e^{j\alpha_m(\phi, \theta)}, \quad (4)$$

where $g_m(\phi, \theta)$ and ψ_m are the amplitude and phase of the complex antenna response and η_m is the phase shift of the carrier on the m -th element which is caused by the propagation distance difference between the m -th element and the reference point. The reference point can be the center or a corner of the PAA. Hence, the steering factor $s_m(\phi, \theta)$ is a complex number embodying the effect of both the antenna response and the DoA information. To simplify the notation, we define $\alpha_m(\phi, \theta) = \psi_m + \eta_m(\phi, \theta)$. $s_m(\phi, \theta)$ is measured in an anechoic chamber by injecting sinusoidal signals to the antenna array from the direction of (ϕ, θ) , where ϕ is scanned manually from 0 to $+2\pi$ and θ from 0 to $+\pi$.

As shown in (3), the received signal on the m -th element is a superposition of the waves from different paths and the noise. By calculating the moving-correlation of $\tilde{y}_m(\tau)$ and the PN-sequence $a(\tau)$ in the delay domain, the result is given by (5), where $\int_0^{T_p} a^2(\tau)d\tau = KP_b$ is the peak value of the auto-correlation function of $a(\tau)$. $N'_m(\tau)$ is the correlation result of $N_m(\tau)$ and $a(\tau)$. As we can see, due to the auto-correlation property of the PN-sequence, the result will generate L peaks at the excess delays of the paths, *i.e.*, τ_l ($l = 1, 2, \dots, L$). One peak in (5) corresponds to an incident path, but it includes both the complex path gain and the steering factor of the receiver antenna array. Therefore, $\tilde{h}_m(\tau)$ is herein called the *observed impulse response (OIR)*.

$$\begin{aligned} \tilde{h}_m(\tau) &= \langle y_m(\tau), a(\tau) \rangle \\ &= \left[\sum_{l=1}^L h_l^{CH} s_m(\phi_l, \theta_l) a(\tau - \tau_l) + N_m(\tau) \right] * a^*(-\tau) \\ &= \sum_{l=1}^L h_l^{CH} s_m(\phi_l, \theta_l) a(\tau - \tau_l) * a^*(-\tau) + N_m(\tau) * a^*(-\tau) \\ &= \sum_{l=1}^L h_l^{CH} s_m(\phi_l, \theta_l) KP_b \delta(\tau - \tau_l) + N_m(\tau) * a^*(-\tau) \\ &= KP_b \sum_{l=1}^L h_l^{CH} s_m(\phi_l, \theta_l) \delta(\tau - \tau_l) + N'_m(\tau). \end{aligned} \quad (5)$$

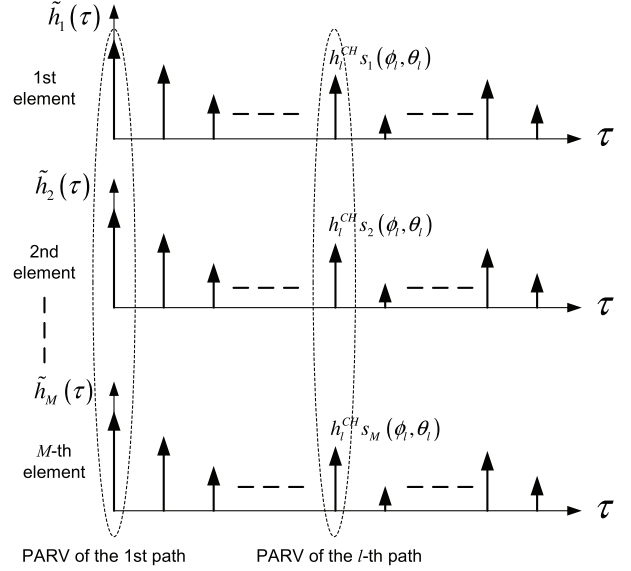


Fig. 1. OIR of M antenna elements and the extraction of the PARVs.

C. DoA Estimation Theory

We organize the complex amplitudes of the L peaks in the m -th OIR, $\tilde{h}_m(\tau)$, in a row vector. Although the analysis in the following is based on an ideal signal model without noise, important insights can be obtained. If the Gaussian noise is ignored, the vector can be expressed as

$$\tilde{\mathbf{a}}_m = KP_b \begin{bmatrix} h_1^{CH} s_m(\phi_1, \theta_1) & h_2^{CH} s_m(\phi_2, \theta_2) & \dots \\ & h_L^{CH} s_m(\phi_L, \theta_L) \end{bmatrix}. \quad (6)$$

The complex amplitudes of the peaks in all the M OIRs from the antenna array can be organized in an $M \times L$ matrix as in (7), shown at the bottom of this page, where the m -th row corresponds to the output of the m -th element and the l -th column contains the OIR of the l -th path on the array. Therefore, one column of $\tilde{\mathbf{A}}$ is called *path array response vector (PARV)* that corresponds to an individual path. The extraction of the PARVs of the paths from the OIRs on the Rx array is illustrated in Fig. 1.

The PARV of the l -th path can be further expressed in a vector notation as

$$\tilde{\mathbf{v}}_l = KP_b \begin{bmatrix} h_1^{CH} s_1(\phi_l, \theta_l) \\ h_1^{CH} s_2(\phi_l, \theta_l) \\ \vdots \\ h_1^{CH} s_M(\phi_l, \theta_l) \end{bmatrix} = KP_b h_l^{CH} \mathbf{s}(\phi_l, \theta_l), \quad (8)$$

where $\mathbf{s}(\phi_l, \theta_l) \triangleq [s_1(\phi_l, \theta_l) s_2(\phi_l, \theta_l) \dots s_M(\phi_l, \theta_l)]^T$ is the M -dimensional *steering vector* pointing toward the DoA of the

$$\tilde{\mathbf{A}} = \begin{bmatrix} \tilde{\mathbf{a}}_1 \\ \tilde{\mathbf{a}}_2 \\ \vdots \\ \tilde{\mathbf{a}}_M \end{bmatrix} = KP_b \begin{bmatrix} h_1^{CH} s_1(\phi_1, \theta_1) & h_2^{CH} s_1(\phi_2, \theta_2) & \dots & h_L^{CH} s_1(\phi_L, \theta_L) \\ h_1^{CH} s_2(\phi_1, \theta_1) & h_2^{CH} s_2(\phi_2, \theta_2) & \dots & h_L^{CH} s_2(\phi_L, \theta_L) \\ \vdots & \vdots & \ddots & \vdots \\ h_1^{CH} s_M(\phi_1, \theta_1) & h_2^{CH} s_M(\phi_2, \theta_2) & \dots & h_L^{CH} s_M(\phi_L, \theta_L) \end{bmatrix}. \quad (7)$$

l -th path. Please note that $\tilde{\mathbf{v}}_l$ is the observed channel measurement where h_l^{CH} , ϕ_l , θ_l , and $\mathbf{s}(\phi_l, \theta_l)$ are unknowns. Our objective is to determine (ϕ_l, θ_l) based on the observed PARV, $\tilde{\mathbf{v}}_l$.

The $M \times M$ covariance matrix of $\tilde{\mathbf{v}}_l$ is calculated as (for easy presentation, the variable tuple (ϕ_l, θ_l) is ignored)

$$\begin{aligned} \tilde{\mathbf{C}}_l &= \tilde{\mathbf{v}}_l \tilde{\mathbf{v}}_l^H = \left| K P_b h_l^{CH} \right|^2 \mathbf{s} \mathbf{s}^H \\ &= \left| K P_b h_l^{CH} \right|^2 \begin{bmatrix} |s_1|^2 & \cdots & s_1 s_M^* \\ \vdots & \ddots & \vdots \\ s_M s_1^* & \cdots & |s_M|^2 \end{bmatrix} \\ &= \left| K P_b h_l^{CH} \right|^2 \begin{bmatrix} g_1^2 & \cdots & g_1 g_M e^{j(\alpha_1 - \alpha_M)} \\ \vdots & \ddots & \vdots \\ g_1 g_M e^{j(\alpha_M - \alpha_1)} & \cdots & g_M^2 \end{bmatrix}, \end{aligned} \quad (9)$$

where $[\cdot]^H$ and $[\cdot]^*$ denote the Hermitian operation and the complex conjugation, respectively, and $s_m(\phi_l, \theta_l)$ is replaced by (4). Obviously, $\tilde{\mathbf{C}}_l$ is a Hermitian matrix.

Lemma 1: The rank of the covariance matrix, $\tilde{\mathbf{C}}_l$, is 1 and the eigenvalues (denoted by λ_m , $m = 1, 2, \dots, M$) satisfy

$$\begin{cases} \lambda_1 &= \left| K P_b h_l^{CH} \right|^2 \sum_{m=1}^M |s_m|^2 \\ &= \left| K P_b h_l^{CH} \right|^2 \sum_{m=1}^M g_m^2(\phi_l, \theta_l), \\ \lambda_2 &= \cdots = \lambda_M = 0, \end{cases} \quad (10)$$

where λ_1 denotes the non-zero eigenvalue.

Proof: See Appendix A. ■

Solving the characteristic equation of $(\lambda \mathbf{I} - \tilde{\mathbf{C}}_l) \mathbf{u} = \mathbf{0}$ where \mathbf{I} denotes the $M \times M$ unit matrix and \mathbf{u} is an $M \times 1$ vector, we can obtain the corresponding eigenvectors \mathbf{u}_m ($m = 1, 2, \dots, M$). Suppose that \mathbf{u}_1 is the eigenvector corresponding to the eigenvalue λ_1 .

Lemma 2: The significant eigenvector, \mathbf{u}_1 , is the steering vector pointing to the DoA of the l -th path, i.e.,

$$\begin{aligned} \mathbf{u}_1 &= [s_1(\phi_l, \theta_l) \ s_2(\phi_l, \theta_l) \ \cdots \ s_M(\phi_l, \theta_l)]^T \\ &= \mathbf{s}(\phi_l, \theta_l). \end{aligned} \quad (11)$$

Proof: See Appendix B. ■

Further, based on the property that $\tilde{\mathbf{C}}_l$ is a Hermitian matrix and $\lambda_1 \neq \lambda_m = 0$ ($m = 2, 3, \dots, M$), we have the following lemma.

Lemma 3: The significant eigenvector, \mathbf{u}_1 (i.e., $\mathbf{s}(\phi_l, \theta_l)$), is orthogonal to the space spanned by the eigenvectors corresponding to the zero-value eigenvalues, i.e., $\mathbf{u}_1 \perp \mathbf{B}_R$ where $\mathbf{B}_R = [\mathbf{u}_2 \ \mathbf{u}_3 \ \cdots \ \mathbf{u}_M]$.

Proof: See Appendix VII. ■

The space based on \mathbf{B}_R is herein termed the *reference subspace* of matrix $\tilde{\mathbf{C}}_l$. Therefore, we can conclude that the steering vector pointing to the l -th path, $\mathbf{s}(\phi_l, \theta_l)$, is orthogonal to the reference subspace. Thus, the *object spatial spectrum* (OSS) is defined with respect to the azimuth-elevation plane as

$$P(\phi, \theta) = \frac{1}{\langle \mathbf{s}(\phi, \theta), \mathbf{B}_R \rangle} = \frac{1}{\mathbf{s}^H(\phi, \theta) \mathbf{B}_R \mathbf{B}_R^H \mathbf{s}(\phi, \theta)}. \quad (12)$$

Due to the orthogonality proved above, we have $\langle \mathbf{s}(\phi, \theta), \mathbf{B}_R \rangle = 0$ when $\phi = \phi_l$ and $\theta = \theta_l$. Consequently, the OSS should generate a peak at the target azimuth-elevation angle. Considering the signal noise in practical field measurements, the DoA of the l -th path can be determined by the 2D peak searching with respect to ϕ and θ jointly. Thus, the estimate is

$$\begin{aligned} (\hat{\phi}_l, \hat{\theta}_l) &= \arg \max_{(\phi, \theta) \in [-\pi, \pi]^2} \{P(\phi, \theta)\} \\ &= \arg \max_{(\phi, \theta) \in [-\pi, \pi]^2} \left\{ \frac{1}{\mathbf{s}^H(\phi, \theta) \mathbf{B}_R \mathbf{B}_R^H \mathbf{s}(\phi, \theta)} \right\}. \end{aligned} \quad (13)$$

As mentioned earlier, $\mathbf{s}(\phi, \theta)$ is measured in advance in an anechoic chamber and \mathbf{B}_R is obtained from the observed PARV. Therefore, the 2D DoA of each resolved propagation path can be estimated using (13) one-by-one independently.

In the DoA estimation of one path, the signals through the other propagation paths are the multipath interference. By using the correlation of the PN-sequences, we can suppress the interference and thus increase the SIR significantly for the DoA estimation. The spread spectrum gain is approximately the length of the PN-sequence, K . Nevertheless, the PN-sequence should not be too short or too long. If it is too short, the spread spectrum gain will be limited. On the other hand, the channel should remain constant during the transmission of the PN-sequence frame as mentioned earlier. Thus its length should be limited and ensure that the transmission time is smaller than the channel coherent time.

Because the OSS of each path is calculated separately and has only one peak, the angular resolution is determined by the minimum AoA/EoA searching step in (13) which equals the angular interval of the array antenna pattern. From this point of view, MAPS has better resolution performance compared with the schemes that generate multi-peak spectra, because the resolution of the latter is twice of the angular interval of the antenna pattern. Furthermore, by using MAPS, even if two paths have the same DoA (delay is different). They may be distinguished first in the time domain by PN-sequence correlation, and then their DoA is estimated. On the other hand, if two paths arrive at the same excess delay (their DoAs are different), they can be separated and estimated in the space domain. The DoA estimation for dense multipath environments will be discussed in details in the next section.

III. EXTENSION OF MAPS FOR DENSE MULTIPATH ENVIRONMENTS

The multipath resolution of the proposed MAPS algorithm in Sec. II depends on the bandwidth of the channel sounding PN-sequences. Therefore, MAPS can work well if the excess delay differences among the propagation paths are larger than the chip duration. However, in dense multipath environments such as indoor channels, the bandwidth of the PN-sequences cannot be increased too much due to the hardware limit. For the case that several paths arrive within the same chip duration or even at the same time, we propose two methods to resolve the paths. One approach is by over-sampling (or interpolation)

of the received signals and successive path deduction in the time-domain, and the other method is spatial smoothing in the space-domain. With these extensions, the MAPS scheme can be used in measurements for dense multipath channels.

A. Over-sampling and Successive Path Deduction

The received signals on the antenna array are sampled by a higher rate than the PN-sequence chip rate. As defined in Sec. II-B, the chip rate of the PN-sequences is $R = 1/T_b$ bps. Suppose that the receiver captures the signals on the antenna array by the sampling rate of IR sps (samples per second). The waveform samples for one PN-sequence duration on the m -th element is denoted by $\tilde{\mathbf{y}}'_m(i)$, $i = 0, 1, 2, \dots, IK - 1$, where each chip duration contains I samples. The local PN-sequence, $a(t)$ as defined in Sec. II-B, is sampled by the chip rate and denoted by $\mathbf{a}(k)$, $k = 0, 1, 2, \dots, K - 1$. The proposed successive deduction approach to extract paths on the m -th antenna element is listed in Algorithm 1.

Algorithm 1. Path Extraction from the Over-Sampled Signal on the m -th Antenna Element

Require: $\tilde{\mathbf{y}}'_m$: over-sampled waveform on the m -th antenna element; \mathbf{a} : PN-sequence;

Ensure: $\tilde{\mathbf{h}}'_m$: estimated CIR;

```

1:  $\tilde{\mathbf{y}}''_m = [\tilde{\mathbf{y}}'_m \tilde{\mathbf{y}}'_m]$ ;
2: for  $i = 0$  to  $IK - 1$  do
3:    $\mathbf{e} = \tilde{\mathbf{y}}''_m(i : I : (K - 1)I + i)$ ;
4:    $\mathbf{f}(i) = \langle \mathbf{a}, \mathbf{e} \rangle$ ;
5: end for
6: for  $i = 1$  to  $KI - 2$  do
7:    $i' = \min\{i + I - 2, KI - 1\}$ ;
8:    $\mathbf{f}(i : i') = \mathbf{f}(i : i') - \mathbf{f}(i - 1)$ ;
9: end for
10:  $\tilde{\mathbf{h}}'_m = \mathbf{f}$ ;
```

Steps 1 to 5 perform the circular correlation between the over-sampled received waveform and the PN-sequence. In Step 3, we extract the i -th ($i = 0, 1, \dots, I - 1$) sample in each chip duration to form a new sequence, \mathbf{e} , whose length is K and equals that of the PN-sequence. Because $\tilde{\mathbf{y}}''_m$ is the concatenation of two sequences of $\tilde{\mathbf{y}}'_m$ in Step 1, \mathbf{e} is actually the sampling of circularly shifted $\tilde{\mathbf{y}}'_m$. Then Step 4 performs the correlation and stores the results in the vector of \mathbf{f} . This correlation result can indicate if there is a new path arriving at this sampling moment. If a path arrives, the correlation should generate a new pulse.

However, the correlation functions calculated with the over-sampled waveforms impinging from different directions (paths) have overlap in the obtained function, \mathbf{f} . Steps 6 to 10 perform the successive deduction of the overlapped correlation results of the paths one-by-one. Because the over-sampling ratio is I , the signal through one path will have non-zero correlation coefficients with the PN-sequence for I times. In other words, its correlation result will affect I samples beginning from the sample when it arrives. Therefore, the correlation results at the time of the $(i - 1)$ -th sample, *i.e.*, $\mathbf{f}(i - 1)$, is deducted from the following $I - 1$ correlation results, as shown in Step 8.

The method by over-sampling and successive path deduction increases the temporal resolution for multipath to be $\Delta\tau = \frac{T_b}{I}$, which is much smaller than that of the original PN-sequence. Thus, the ability to resolve dense multipaths in time-domain is improved significantly.

B. Spatial Smoothing on PARVs

If two or more paths arrive at the receiver within a sampling interval or at the same time, they cannot be separated in the time-domain. To address this issue, we further extend the MAPS algorithm with spatial smoothing to resolve paths in the space domain.

We consider that there are L propagation paths and the antenna array size is M elements. Without loss of generality and for easy presentation, we suppose that the first and second paths arrive at the receiver at the same time, *i.e.*, at the excess delay of $\tau_{1,2}$. Since the PN-sequences through the first and second paths arrive at the same time, their correlations with the local PN-sequence are added together. Consequently, the correlation result between the received waveform on the m -th antenna element and the PN-sequence in (5) in Sec. II-B becomes

$$\begin{aligned} \tilde{h}_m(\tau) = & K P_b \left[h_1^{CH} s_m(\phi_1, \theta_1) + h_2^{CH} s_m(\phi_2, \theta_2) \right] \delta(\tau - \tau_{1,2}) \\ & + K P_b \sum_{l=3}^L h_l^{CH} s_m(\phi_l, \theta_l) \delta(\tau - \tau_l) + N'_m(\tau). \end{aligned} \quad (14)$$

Then, the peak values of the OIR on the m -th element in (6) in Sec. II-C becomes

$$\begin{aligned} \tilde{\mathbf{a}}_m = & K P_b \left[h_1^{CH} s_m(\phi_1, \theta_1) + h_2^{CH} s_m(\phi_2, \theta_2) \right. \\ & \left. h_3^{CH} s_m(\phi_3, \theta_3) \quad \dots \quad h_L^{CH} s_m(\phi_L, \theta_L) \right]. \end{aligned} \quad (15)$$

The PARV which contains the channel responses of both the first and second paths on the M elements can be expressed as

$$\begin{aligned} \tilde{\mathbf{v}}_{1,2} = & K P_b \begin{bmatrix} h_1^{CH} s_1(\phi_1, \theta_1) + h_2^{CH} s_1(\phi_2, \theta_2) \\ h_1^{CH} s_2(\phi_1, \theta_1) + h_2^{CH} s_2(\phi_2, \theta_2) \\ \vdots \\ h_1^{CH} s_M(\phi_1, \theta_1) + h_2^{CH} s_M(\phi_2, \theta_2) \end{bmatrix} \\ = & K P_b \left[h_1^{CH} \mathbf{s}(\phi_1, \theta_1) + h_2^{CH} \mathbf{s}(\phi_2, \theta_2) \right]. \end{aligned} \quad (16)$$

Now we introduce the spatial smoothing method to separate the two paths in the space domain. First, the elements from the 1st to $(M - 1)$ -th rows of $\tilde{\mathbf{v}}_{1,2}$ are selected and form a new vector, denoted by $\tilde{\mathbf{v}}'_{1,2}$. The elements from the 2nd to M -th rows of $\tilde{\mathbf{v}}_{1,2}$ form another vector, denoted by $\tilde{\mathbf{v}}''_{1,2}$. Second, the covariance matrices of $\tilde{\mathbf{v}}'_{1,2}$ and $\tilde{\mathbf{v}}''_{1,2}$ are calculated independently by

$$\begin{cases} \tilde{\mathbf{C}}'_{1,2} = \tilde{\mathbf{v}}'_{1,2} (\tilde{\mathbf{v}}'_{1,2})^H, \\ \tilde{\mathbf{C}}''_{1,2} = \tilde{\mathbf{v}}''_{1,2} (\tilde{\mathbf{v}}''_{1,2})^H. \end{cases} \quad (17)$$

Since $\tilde{\mathbf{v}}'_{1,2}$ and $\tilde{\mathbf{v}}''_{1,2}$ are vectors, we have $\text{rank}\{\tilde{\mathbf{v}}'_{1,2}\} = \text{rank}\{\tilde{\mathbf{v}}''_{1,2}\} = 1$. Similar to the proof in Appendix A, we can get $\text{rank}\{\tilde{\mathbf{C}}'_{1,2}\} = \text{rank}\{\tilde{\mathbf{C}}''_{1,2}\} = 1$. Then, the combined covariance matrix is obtained by

$$\tilde{\mathbf{C}}_{1,2} = \frac{\tilde{\mathbf{C}}'_{1,2} + \tilde{\mathbf{C}}''_{1,2}}{2}, \quad (18)$$

and it can be proved that $\text{rank}\{\tilde{\mathbf{C}}_{1,2}\} = 2$.

Then the singular value decomposition (SVD) is performed on $\tilde{\mathbf{C}}_{1,2}$ which has two significant eigen values (denoted by λ_1 and λ_2) and the other eigenvalues are close to zero ($\lambda_m \approx 0$ for $m = 3, 4, \dots, M$). The two eigenvectors corresponding to the significant eigenvalues are denoted by \mathbf{u}_1 and \mathbf{u}_2 , and the other eigenvectors span the reference subspace, *i.e.*, $\mathbf{B}_R = [\mathbf{u}_3 \mathbf{u}_4 \dots \mathbf{u}_M]$. According to Appendix B, \mathbf{u}_1 and \mathbf{u}_2 are actually the steering vectors pointing to the DoAs of the first and second paths, and they are both orthogonal to \mathbf{B}_R . Finally, the spatial spectrum is calculated by (12) in Sec. II-C using the steering vector $\mathbf{s}(\phi, \theta)$ and the reference subspace \mathbf{B}_R obtained above. The OSS should have two peaks which indicate the DoAs of the two paths. Therefore, the estimates, $(\hat{\phi}_1, \hat{\theta}_1)$ and $(\hat{\phi}_2, \hat{\theta}_2)$, are obtained simultaneously by (13) in one iteration. The spatial smoothing approach presented above can readily be extended to separate three or more paths if the antenna array size is larger.

In summary, we have proposed two extensions to the original MAPS scheme. The first method is by over-sampling and successive path deduction, which can increase the temporal resolution of the OIR by I times than the original PN-sequence where I is the over-sampling ratio. Thus, the ability to resolve dense multipaths in time domain is improved significantly. The second method is to perform spatial smoothing on the PARVs and the paths arriving at the same time can be separated and estimated in the space domain. These two methods can be used jointly to resolve paths in the time-space domain. Thus, even if paths have the same ToA or DoA, they can be separated and estimated.

IV. MAPS ALGORITHM IMPLEMENTATION

In a channel measurement system equipped with a receiver PAA, the MAPS algorithm is implemented in two stages based on the theoretical framework derived in the previous sections. In the first stage, the OIR matrix is extracted from the captured waveforms and, in the second stage, the 2D DoAs of all the identified paths are estimated sequentially. The operation is summarized in Algorithm 2, where there may be one or two paths arriving within a sampling interval. It can be easily extended to estimate more paths in one sampling interval. Suppose the power threshold for a valid path is P_0 , and the paths whose power is below P_0 are ignored.

Algorithm 2. Steps of DoA estimation in MAPS

Require: Waveforms captured on the M antenna array elements with over-sampling ratio of I , $\tilde{\mathbf{y}}'_m$, $m = 1, 2, \dots, M$;

Ensure: AoAs and EoAs of all propagation paths, $(\hat{\phi}_l, \hat{\theta}_l)$, $l = 1, 2, 3, \dots$;

- 1: **for** $m = 1$ to M **do**
 - 2: Perform successive path deduction to obtain the OIR sequence, $\tilde{\mathbf{h}}'_m$, from the received waveforms $\tilde{\mathbf{y}}'_m$ using Algorithm 1;
 - 3: Put the complex amplitudes of the peaks whose power is larger than P_0 in $\tilde{\mathbf{h}}'_m$ into a vector, $\tilde{\mathbf{a}}_m$ (suppose there are L peaks);
 - 4: **end for**
 - 5: Organize the OIR matrix, $\tilde{\mathbf{A}}$, according to (7);
 - 6: **for** $l = 1$ to L **do**
 - 7: Extract the PARV of the l -th path, $\tilde{\mathbf{v}}_l$, from $\tilde{\mathbf{A}}$ (*i.e.*, the l -th column);
 - 8: Construct the covariance matrices, $\tilde{\mathbf{C}}'_l$, $\tilde{\mathbf{C}}''_l$, and $\tilde{\mathbf{C}}_l$ according to (17) and (18);
 - 9: Perform SVD on $\tilde{\mathbf{C}}_l$ and obtain the reference subspace, \mathbf{B}_R , according to Lemma 3;
 - 10: Calculate the OSS $P(\phi, \theta)$ by (12) where the steering vector $\mathbf{s}(\phi, \theta)$ scans over the 2D antenna pattern;
 - 11: Obtain the AoA and EoA estimates of one or two paths, by searching the peak(s) of $P(\phi, \theta)$ according to (13);
 - 12: **end for**
-

Compared with the methods such as MUSIC that generate multi-peak spectra, more iteration loops are needed in MAPS. However, the computations are mainly the linear calculations on PARVs and their covariance matrices, instead of the RF signal samples. Furthermore, the dimensions of the matrices equal the antenna array size and thus are usually small due to the hardware constraint. Therefore, the matrix operations in MAPS have a much less computational complexity compared with the traditional methods. In addition, the MAPS algorithm has no requirement for the shape of the PAA and can be applied to arbitrary 2D arrays which have at least 2 elements in horizontal and vertical dimensions.

V. PERFORMANCE SIMULATION AND COMPARISON

A. Simulation Setting

In this section, the multipath DoA estimation is simulated with various received SNR, number of propagation paths, and antenna array sizes. The estimation error and angular resolution of MAPS, MUSIC, CAPON, ESPRIT, MP, and SAGE are presented for comparison.

Static multipath propagation channels with additive white Gaussian noise are simulated. In the simulations of all algorithms, the same PN-sequence of 1,023 bits is adopted as the baseband signal. Two sequences plus a cyclic prefix and post-fix form a frame and the repetition of the frames are modulated on the carrier of 25 KHz via BPSK with a bandwidth of 2.5 KHz, and transmitted through the channel. The received signal is the superposition of the electric waves that arrive at the Rx with different delay, power, and incident directions through the propagation paths. The received RF signal is sampled at a 50 KHz over-sampling rate and stored for post-processing. In the simulations, the antenna elements are omnidirectional and spaced by half a wavelength. The resolution of the antenna pattern diagram (steering vector) is 1° . The input signals for all the simulated algorithms are the same (*i.e.*, the samples of the

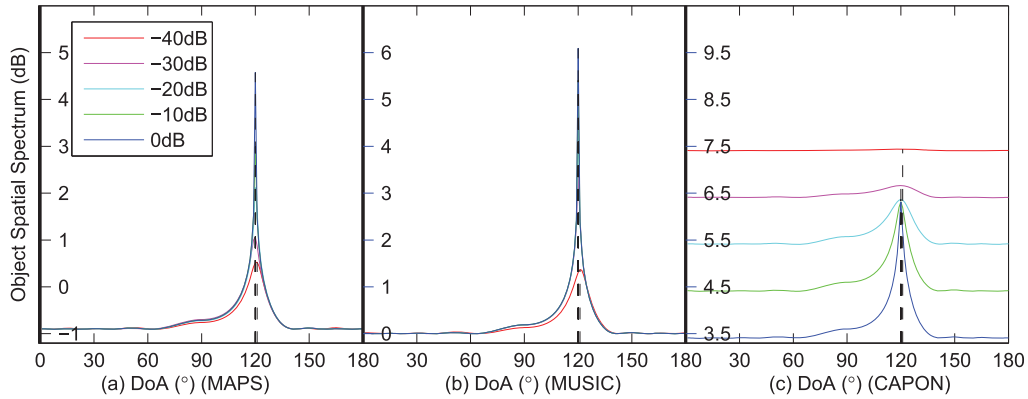


Fig. 2. Spatial spectra of three algorithms with different SNRs.

received RF signal on each antenna element). If not specified, the excess delay and incidence angles of the paths are random in the simulation trials.

To evaluate the estimation accuracy, we define the root mean square error (RMSE) of the 2D DoA estimate as

$$\varepsilon_l = \sqrt{(\phi_l - \hat{\phi}_l)^2 + (\theta_l - \hat{\theta}_l)^2}, \quad (19)$$

where (ϕ_l, θ_l) is the true DoA of the l -th path and $(\hat{\phi}_l, \hat{\theta}_l)$ is the estimation result. For each performance evaluation, simulations have been conducted for more than 10 times and the results are consistent. The spatial spectra presented in the figures in this section are randomly selected from the simulation results.

B. DoA Estimation with Different SNRs

First, to compare the performance more clearly, the DoA estimation results of the algorithms in one dimension (*e.g.*, azimuth) are presented. The results in the other dimension have the same trend. Suppose that one propagation path arrives from the AoA of 120° . We use a horizontal linear antenna array (LAA) with 8 elements. The signal SNR varies from -40 to 0 dB with a step size of 10 dB. The obtained spectra are plotted in Fig. 2. As can be seen, both MAPS and MUSIC can provide accurate results ($\varepsilon_l = 0^\circ$) and their spectra are sharp, even with SNR of -40 dB. CAPON fails to identify the DoA with SNR below -30 dB.

Second, we have performed simulations of MAPS with SNRs of -30, -15, and 0 dB and the cumulative distribution functions (CDFs) of the RMSE are obtained. Suppose that there are three paths. With each SNR, the simulations are run for 300 times. In each simulation trial, the incidence angles and delay of the paths are random, and the average RMSE of the estimation results of the three paths are calculated. The empirical CDFs of the average RMSE are plotted in Fig. 3. The figure further demonstrates the performance of the MAPS algorithm with different SNR.

Third, the 2D DoA estimation by MAPS is simulated using a 4×4 square PAA and 3 incident paths. The obtained 2D OSSs are plotted in Fig. 4 with the received SNR of 0, -15, and -35 dB. Although the OSS of each path is calculated individually in MAPS, we superimpose them together in the figures for easier

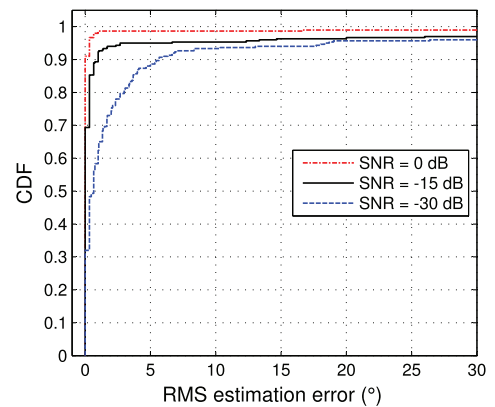


Fig. 3. Empirical CDF of the RMSE in DoA estimations for three paths.

illustration (the same presentation approach is adopted in the other figures in this section). Although the peaks become lower and wider as the SNR decreases, they can indicate the DoAs accurately ($\varepsilon_l = 0^\circ$ for $l = 1, 2, 3$).

The results demonstrate that MAPS has a comparable SNR performance with MUSIC but has a much lower computational complexity. This is mainly because MAPS estimates the DoAs using the PARVs instead of the original RF signal samples. Since the PARVs are obtained by the correlation of the PN-sequence, the computational complexity is reduced significantly without loss of signal power (or SNR).

C. DoA Estimation with Different Array Sizes

We first compare the estimation results in one dimension of the algorithms, where an Rx LAA in the azimuth dimension is used and its size changes from 2 to 8 elements. There is only one path with the AoA of 120° and SNR of 0 dB. The spatial spectra are plotted in Fig. 5, which shows that MAPS and MUSIC both have sharp peaks with errors of $\varepsilon_l = 0^\circ$.

Then, we use the PAA with sizes of 4×4 , 3×3 , and 2×2 , to perform 2D DoA estimation by MAPS. Three paths impinge at the Rx and the resulting OSSs are shown in Fig. 6. The DoA estimation errors are $\varepsilon_l = 0^\circ$ for $l = 1, 2, 3$. Obviously, the change of PAA size does not lead to a significant performance degradation. Therefore, because of its good adaptability to the antenna array size, MAPS can be applied to field channel

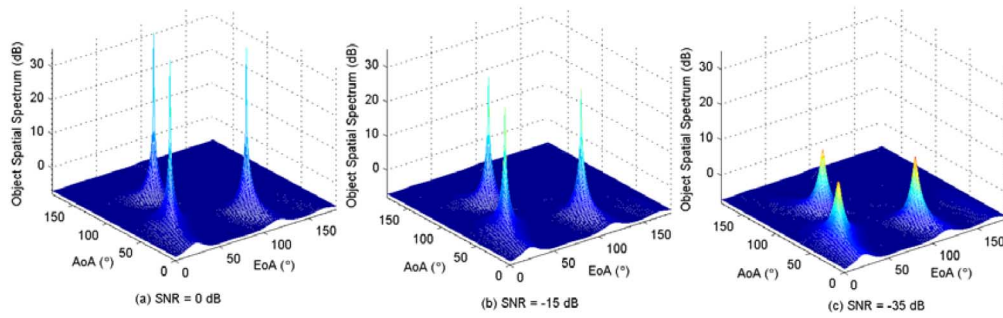


Fig. 4. 2D spatial spectra with different SNRs using MAPS.

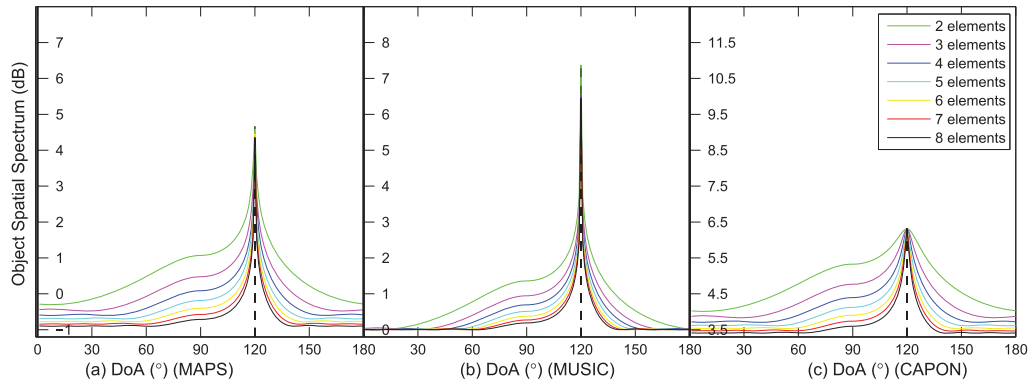


Fig. 5. Spatial spectra of three algorithms with different array sizes.

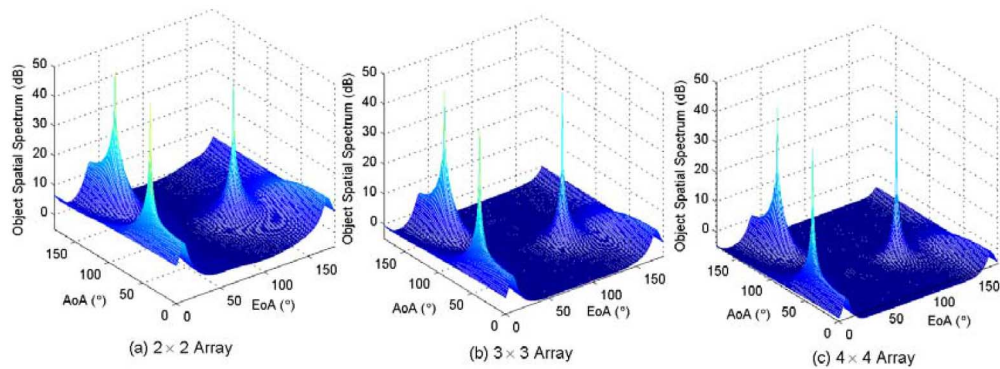


Fig. 6. 2D spatial spectra with different array sizes using MAPS.

measurements especially when the antenna array size is limited (the hardware cost can be reduced).

D. DoA Estimation with Different Number of Paths

In this simulation, the scenario is considered where a large number of incident paths are present. For example, we use a horizontal LAA consisting of 5 elements and the SNR is set to 20 dB. MUSIC and CAPON are limited in that an antenna array with M elements in one dimension can estimate $M - 1$ DoAs at most. Therefore, in the simulations, 4 propagation paths exist and the AoAs are 70° , 80° , 90° , and 100° . The obtained spectra are plotted in Fig. 7(b) and (c). Both of these methods fail to recognize the target angles.

In contrast, the number of estimated DoAs can be unlimited in MAPS. Therefore, in the simulation of MAPS, we generate 15 paths with different incidence angles. The spectra

of all paths are superimposed in Fig. 7(a), which shows that the incidence angles are all precisely distinguished ($\varepsilon_l = 0^\circ$ for $l = 1, 2, \dots, 15$). The virtue of MAPS is mainly because the paths are first separated by the PN-sequence response in the OIR and then their DoAs are estimated individually and independently. Therefore, the limitation in the number of DoAs is avoided.

For 2D DoA estimation by MAPS, we use a 3×3 PAA and set the SNR to be 0 dB. A total of 4, 8, and 12 paths impinge at the Rx with different AoAs and EoAs. The obtained 2D OSSs are plotted in Fig. 8, where all the peaks can be easily identified.

To estimate a large number of propagation paths in practical channel measurements, traditional algorithms require a large Rx antenna array. Nevertheless, the proposed MAPS scheme avoids this requirement by using scaling in the time domain to obtain scaling in the spatial domain.

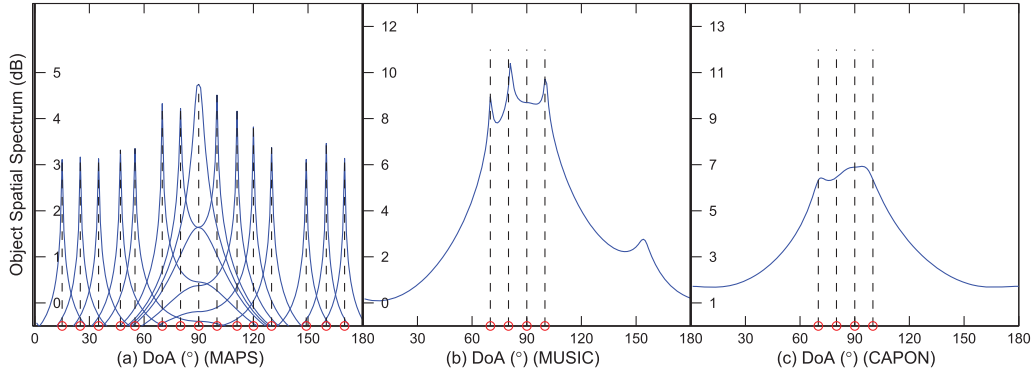


Fig. 7. Spatial spectra of three algorithms with multiple incidence angles.

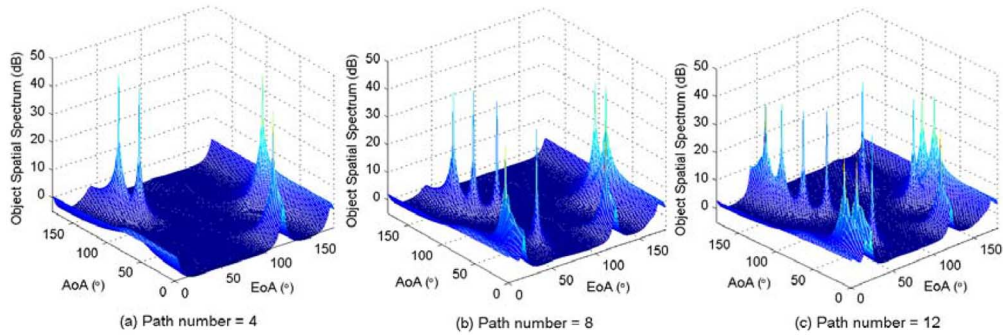


Fig. 8. 2D spatial spectra with multiple incidence angles.

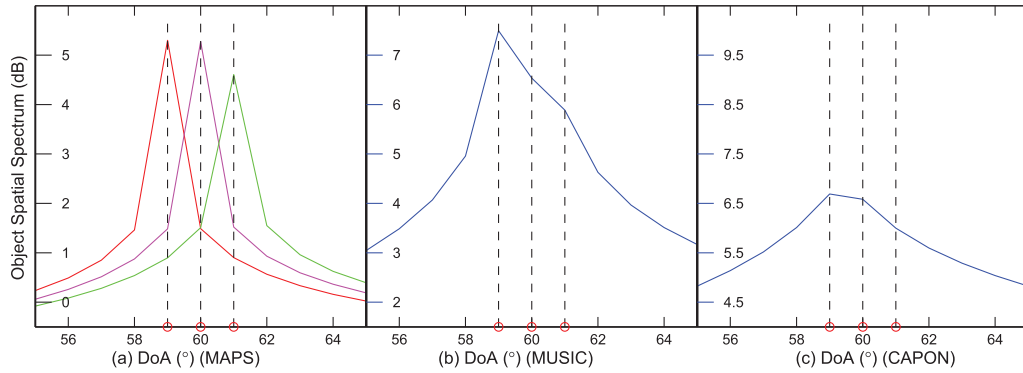


Fig. 9. Spatial spectra of three algorithms for three close incidence angles.

E. DoA Estimation Resolution

Another important performance metric is angular resolution, *i.e.*, the minimum gap between two incidence angles that can be distinguished. Here, we assume that the resolution of the directional antenna pattern of the PAA is 1° , which is the lower bound (best resolution) in the angular estimation. For multiplexing algorithms, such as MUSIC and CAPON, the best resolution is 2° as a gap must be present between two peaks in the obtained spectrum. In ESPRIT and MAPS, however, since the spectra for paths are separated and the spectrum for each path has only one peak, the estimation resolution can be 1° .

In the simulations, the PAA size is $M = 8$ and SNR is 10 dB. Three propagation paths have incidence angles of 59° , 60° , and 61° . The estimation results are shown in Fig. 9. Although

MUSIC and CAPON both generate spectrum peaks around the target angles, the three paths are difficult to distinguish. Nevertheless, MAPS can identify their DoAs clearly (Fig. 9(a)). Since MAPS first resolves the paths in the time domain by high-resolution channel sounding using the PN-sequences, their DoAs are estimated separately. In this way, MAPS actually uses the high temporal resolution in the time-domain channel sounding to achieve the high angular resolution in the space domain.

F. Multipath Interference Suppression

In the DoA estimation of one propagation path, the signals through the other paths are the interference that can

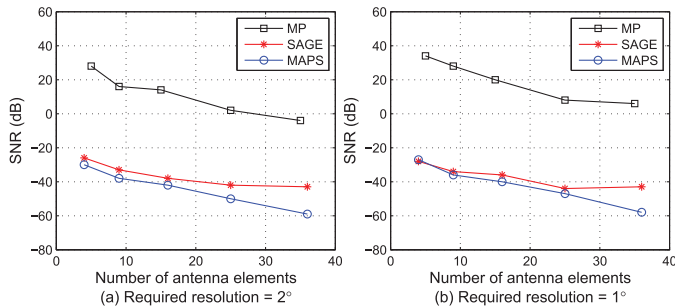


Fig. 10. Minimum SNR required to distinguish two paths.

severely degrade the estimation accuracy. Therefore, suppressing the multipath interference is critical in the DoA estimation for channel measurements. In this simulation, the metric is the minimum SNR required to successfully distinguish two paths, given the DoA difference and the antenna array. Since the estimation accuracy depends on both noise and interference, an algorithm that requires a lower SNR should have better multipath interference suppression, and vice versa.

The proposed MAPS algorithm is based on the subspace-decomposition (covariance matrix) techniques. In this subsection, we selected another two kinds of algorithms for performance comparison, MP [12] and SAGE [26]. The one and two dimensional MP algorithms work with the received signals directly without forming a covariance matrix and can find the DoAs of coherent sources using a single snapshot. The SAGE algorithm has been widely adopted to do parameter estimations for multipath propagation measurements. As mentioned in Sec. I, SAGE performs iterative joint EM estimation on multiple path parameters like the excess delay, incidence angle, Doppler frequency, and power of the impinging waves. The MP and SAGE algorithms are both designed to work with correlated signals.

First, we set the angular difference of two paths to be 2° in one dimension. The minimum SNR required to distinguish the two paths is plotted in Fig. 10(a). As expected, the required SNR decreases with increased array size. MAPS outperforms the other two schemes by requiring smaller SNR. The SNR for SAGE is slightly larger than MAPS, but it requires much higher computational complexity. The SNR for MP is much higher. This may be because MP just utilizes a single snapshot but SAGE and MAPS use all the snapshots within one PN-sequence duration. Therefore, the low SNR is compensated by a large number of snapshots in the time domain in these two schemes.

Second, we change the difference between the two paths to 1° and the results are plotted in Fig. 10(b). Compared to Fig. 10(a), the required SNR increases because higher estimation accuracy is needed. Again, the SNR for MAPS is lower than that of the other two schemes.

This simulation illustrates that the spread spectrum gain leads to a much higher signal-to-interference ratio (SIR) in the obtained PARVs for DoA estimation in MAPS. This virtue is important for measuring intensive multipath channels where the interference among MPCs is severe.

G. Over-sampling and Successive Path Deduction

In this subsection, simulations are conducted to verify the path deduction method presented in Sec. III-A. We suppose that three paths arrive within one chip duration, at the moments of $0.1T_b$, $0.3T_b$, and $0.7T_b$ where T_b is the chip duration of the PN-sequence as defined in Sec. II-B. The paths arrive with the DoAs of 60°, 90°, and 100°. Their power normalized with respect to the first path is 1, 0.7, and 0.4. The received SNR is 5 dB. We utilize an LAA with the size of 8 elements. As specified in Sec. V-A, the over-sampling ratio is 20, which means that there are 20 samples per chip in the received signals. The simulation results for the path separation and DoA estimations are plotted in Fig. 11.

Fig. 11(a) shows the correlation result between the received signal on one antenna element and the PN-sequence. Since the three paths arrive within one chip duration, their correlation functions have overlap. By using the proposed successive deduction method (Algorithm 1), the impulse responses of the paths are separated, as plotted in Fig. 11(b). Their power and delay are correctly identified. Finally, the DoAs of the paths are estimated using MAPS and the spatial spectra are plotted together in Fig. 11(c). As can be seen, the DoAs are estimated successfully.

This simulation verifies that the proposed successive path deduction method with over-sampling can correctly resolve paths which arrive within one chip duration. The time resolution is improved to be $\Delta\tau = \frac{T_b}{I}$. Therefore, the resolution for path separation is significantly increased.

H. Spatial Smoothing Method

In this subsection, simulations are conducted to verify the spatial smoothing method in MAPS proposed in Sec. III-B. We suppose that two paths arrive at the same moment of $0.5T_b$ and at the DoAs of 25° and 70°. Their power normalized with respect to the first path is 1 and 0.5. The received SNR is 10 dB. The sampling rate is the same as the chip rate of the PN-sequence. In other words, the received signals have 1,023 samples for a whole PN-sequence duration and one sample for each chip. We utilize an LAA with the size of 4 or 6 elements. The obtained spatial spectra obtained by the two antenna arrays are plotted in Fig. 12. As can be seen, the two paths are separated and their DoAs are estimated accurately.

VI. FIELD MEASUREMENT TESTS

A. Channel Sounder Implementation

A 3 D spatial channel sounder, using the proposed MAPS scheme, was implemented by the joint efforts of Huawei Technologies Ltd. and the Northwestern Polytechnical University (NPU). The sounder consists of a receiver (Rx) and a transmitter (Tx) (Fig. 13(a) and (b)) and is designed based on the direct-sequence-spread-spectrum (DSSS) transmission scheme as described in Sec. II-B. A PN-sequence with the length of $N = 1,023$ bits and a bandwidth of 62.5 MHz is generated periodically by an Agilent 81150 A waveform generator.

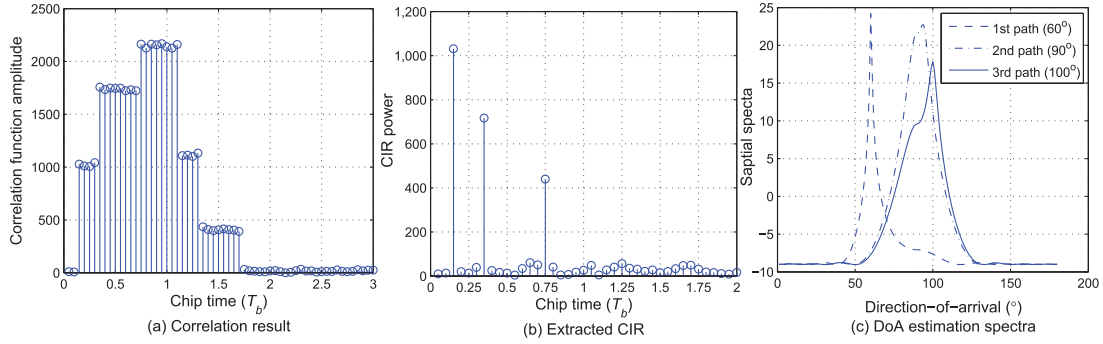


Fig. 11. DoA estimation of paths arriving within one chip duration.

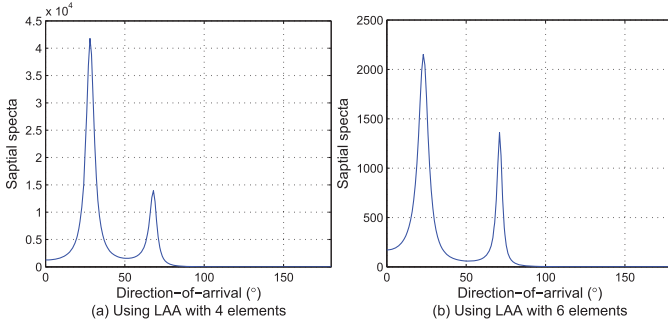


Fig. 12. DoA estimation of paths arriving at the same time.



Fig. 14. DoA estimation experiment setting on a square.

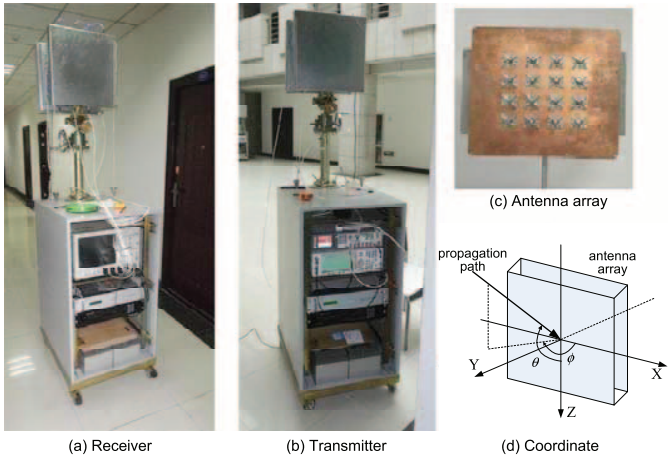


Fig. 13. The spatial channel sounder and the coordinate system for DoA defined with respect to the Rx antenna array.

One sequence lasts for $16.368 \mu\text{s}$. The sequences are modulated via BPSK on the carrier of 2.6 GHz by an Agilent E4438C vector signal generator. The RF signal is then processed by a bandpass filter and amplifier and transmitted.

Both the Tx and Rx are equipped with a 4×4 square array of patches. Each patch consists of two dipole antenna elements with $\pm 45^\circ$ polarizations (Fig. 13(c)). Each antenna element has 7 dBi gain and a half-power beamwidth of -70° to $+70^\circ$ in both azimuth and elevation dimensions. The spacing between the rows and columns is 0.5 wavelength. Thus, the 32 antenna elements form two 4×4 square arrays in $+45^\circ$ and -45° polarizations. The $+45^\circ$ array is used in the measurements in this work.

The antenna elements work in a time division multiplexing (TDM) manner. On the Tx side, an electrical switch with 1 input port and 32 output ports is connected to the 32 antenna elements, so that they are stimulated one-by-one sequentially and each transmits for 1 ms. On the Rx side, the 32 elements are divided into 8 groups and the 4 elements in one column with the same polarization belong to one group. An electrical switch with 32 input and 4 output ports is connected to the array, which selects one group and outputs the received signals to 4 sets of radio front end (FE) including low noise amplifiers (LNAs) and bandpass filters. The signals are then directly input into the 4 radio ports of a Tektronix DSA70604B oscilloscope for sampling, so that the received signals of one group are captured simultaneously. Each group is connected for signal capture for 0.1 ms and the 8 groups are switched circularly. Thus, during the transmission of one Tx antenna element, each of the 32 Rx elements can receive a complete frame of the PN-sequences.

Two GPS rubidium clocks are equipped on the Tx and Rx systems to provide synchronized clocks for the signal generation, capture, and antenna switching. The 3 D directional pattern of the antenna arrays have been measured in an anechoic chamber with the angular interval of 1° in both azimuth and elevation dimensions.

B. Measurement Test on a Square

To validate the proposed MAPS algorithm, propagation measurements were performed on an open square so as to have a clean LOS path with controlled DoA. The test setup is shown in Fig. 14. The Tx and Rx PAAs were both 2.09 m high and the

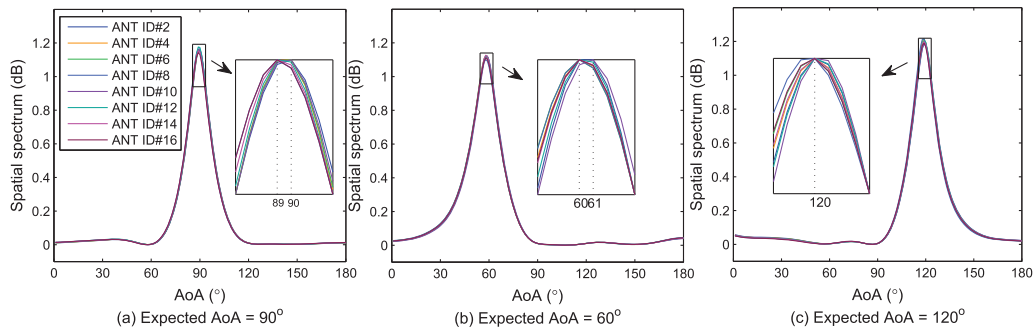


Fig. 15. Spatial spectra for AoA estimation of square measurement data.

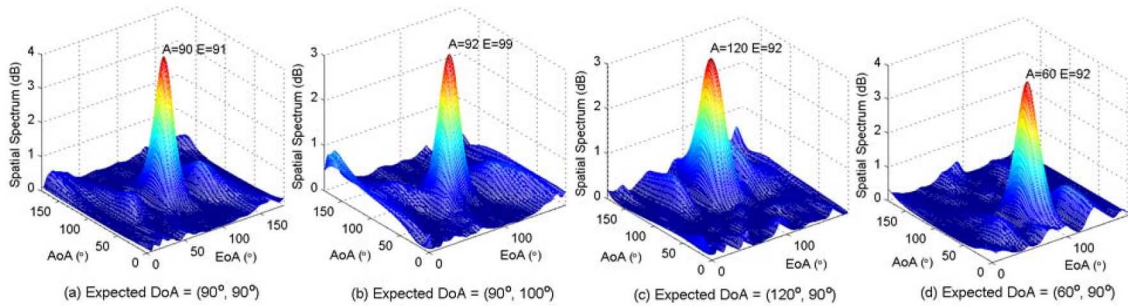


Fig. 16. 2D spatial spectra for DoA estimation of square measurement data.

horizontal distance was 8 m. The coordinate for the incident waves on the Rx PAA was defined as illustrated in Fig. 13(d). At first, the two PAAs were face to face so that the AoA and EoA of the LOS path should be both 90° . Then the Rx array was rotated horizontally by $\pm 30^\circ$ and vertically by -10° , to change the incidence angle. In our measurements, the transceivers were stationary and the environment was static. Hence the channel was time-invariant during a receiving cycle of the 8 groups (0.8 ms). For each Rx PAA rotation, the 32 Tx elements transmitted one-by-one for one cycle. Thus we captured 32 channel snapshots (*i.e.*, 32 samples of the array channel response) independently. Then the DoA of the LOS path was estimated for each snapshot using MAPS.

We first analyze the estimation results of the AoA. We randomly select 8 samples of the channel snapshots which were obtained by different Tx antenna elements. The azimuth OSSs obtained by MAPS are plotted together in Fig. 15 with the Rx PAA rotated horizontally to the three angles mentioned above. As can be observed, the obtained OSSs for all the 8 channel snapshots are well coincident. For the AoA of 90° , the estimation results of 4 measurements were 90° and the others were 89° . For the AoA of 60° , the estimation results of 7 measurements were 60° and the other one was 61° . Finally, for the AoA of 120° , the results of all of the 8 measurements were 120° . In summary, 79% tests obtained accurate estimates and 21% of the tests had $\varepsilon_1 = 1^\circ$ error.

We then evaluated the 2D DoA estimation performance when the incidence angle of the LOS path was $(90^\circ, 90^\circ)$, $(90^\circ, 100^\circ)$, $(120^\circ, 90^\circ)$, and $(60^\circ, 90^\circ)$. The obtained 2D OSSs are plotted in Fig. 16, where the maximum estimation error is $\varepsilon_{\max} = 2.2^\circ$. The error may be caused by the noise in

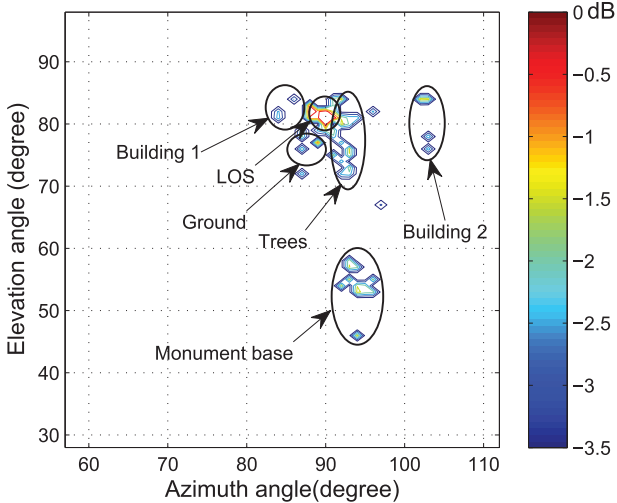
the system and the random deviation in the rotated angles of the Rx PAA.

C. Measurement Test in Street Canyon Environment

We conducted a field spatial channel measurement to validate the effectiveness of MAPS. The experiment was conducted in a typical LOS street canyon environment on the campus of NPU. The Rx was installed on the top of a 5-floor office building and the center of the PAA panel was 24.5 m above the ground. The Tx was placed in a street in front of the Rx at a horizontal distance of 136 m. On both sides of the street were 5-floor office buildings and the width of street was 27 m.

The power of the identified propagation paths impinging on the Rx PAA is plotted in the azimuth-elevation plane in Fig. 17(a) according to their 2D DoAs estimated by MAPS. The power profile is superimposed in the street photo which was taken from the Rx antenna in Fig. 17(b) (the camera was placed at the center of the Rx antenna panel).

In Fig. 17, the intensive clustered MPCs can be seen and the spatial power profile is analyzed as follows. The MPC with the highest power (red color) arrived with EoA of about 81° and AoA of about 90° . This cluster can be identified as the LOS path as it had the strongest propagation power and was received from the Tx direction. The two clusters on both sides of the LOS path, whose EoAs were concentrated around 84° and 103° , should be reflections from the buildings on the street sides. Since they were reflected on the walls of the two 5-floor buildings, their EoAs would be higher than the LOS path from the Tx on the ground. The cluster that was slightly below the LOS path in Fig. 17 should be the reflection from the ground.



(a) Power profile in the azimuth-elevation plane (the power of MPCs is normalized by the strongest MPC).



(b) Estimated 2D power profile received at the Rx.

Fig. 17. Estimated 2D power profile of the MPC clusters in a street canyon environment.

Because the height of the Tx was much closer to the ground than the Rx, the reflection point on the ground should be close to the Tx and hence the EoA of the ground reflection should be slightly smaller than that of the LOS path. The clusters to the right of the LOS path were the MPCs scattered from the foliage of the trees besides the Tx in the middle of the street. These trees were aligned parallel to the street. Therefore, the EoAs of these MPCs should be slightly lower than that of the LOS path and along the line of the trees, as observed in Fig. 17. Finally, the lowest cluster were from the scattering on the surface of the monument base in front of the Rx.

The estimated DoAs of the MPCs appear to match well with the spatial propagations as expected according to the scattering environment. The experiments in this section validate that the proposed MAPS scheme is effective in practical spatial channel measurements.

VII. CONCLUSION

In this paper, a new 2D DoA estimation scheme, named MAPS, is proposed for multipath propagation characterization. Differing from traditional methods, MAPS uses the temporal channel response of PN-sequences received by an arbitrary 2D

PAA. The PARV of each path is first extracted from the array response and then the DoAs of the MPCs are estimated sequentially and independently. MAPS can estimate a large number of DoAs of propagation paths, which is not limited by the antenna array size or affected by the correlation among multipath signals. Furthermore, the PN-sequence correlation operation in MAPS can effectively suppress the multipath interference, so that the spread spectrum gain can significantly increase the accuracy of the DoA estimation. MAPS has been compared with other algorithms such as MUSIC, ESPRIT, and SAGE by simulations. The results have shown that MAPS outperforms the conventional methods in estimation accuracy and capacity (number of DoAs to estimate) for various SNRs, antenna array sizes, numbers of paths, and delay differences. Furthermore, a channel sounder using the MAPS scheme has been developed and the field channel measurement tests have verified that the proposed MAPS scheme is able to estimate multipath DoAs in realist channels with low hardware and software complexity. Using the channel sounder, field channel measurement campaigns are currently undergoing [27]–[29]. Extending MAPS to characterize the multipath propagations from multiple sources simultaneously is an important issue to address, especially for the study of channel spatial correlation properties. Moreover, applying MAPS to the 3D cooperative localization in wireless networks is also an interesting topic.

ACKNOWLEDGEMENT

This work was partly supported by NSFC (61202394, 61571370), Natural Science Basic Research Plan in Shaanxi Province (2015JM6349), Fundamental Research Funds for the Central Universities (3102014KYJD033), Foundation for Selected Overseas Chinese Scholars, and Natural Sciences and Engineering Research Council of Canada.

APPENDIX A

PROOF OF THE RANK AND EIGENVALUES OF $\tilde{\mathbf{C}}_l$

In Sec. II-C, $\tilde{\mathbf{C}}_l$ is the covariance matrix of the l -th path's PARV as defined in (9). Since $\tilde{\mathbf{C}}_l = \tilde{\mathbf{v}}_l \tilde{\mathbf{v}}_l^H$, we have $\text{rank}\{\tilde{\mathbf{C}}_l\} \leq \min\{\text{rank}\{\tilde{\mathbf{v}}_l\}, \text{rank}\{\tilde{\mathbf{v}}_l^H\}\}$. As $\tilde{\mathbf{v}}_l$ is a vector and $\text{rank}\{\tilde{\mathbf{v}}_l\} = \text{rank}\{\tilde{\mathbf{v}}_l^H\} = 1$, we have $\text{rank}\{\tilde{\mathbf{C}}_l\} \leq 1$. Moreover, because $\tilde{\mathbf{C}}_l$ is a non-zero matrix and thus its rank should be larger than 0, it can be concluded that $\text{rank}\{\tilde{\mathbf{C}}_l\} = 1$.

As defined in Sec. II-C, the eigenvalues of $\tilde{\mathbf{C}}_l$ are $\lambda_1, \lambda_2, \dots, \lambda_M$. Let $c_{i,j}$ ($i = 1, 2, \dots, M, j = 1, 2, \dots, M$) denote the element in the i -th row and j -th column in $\tilde{\mathbf{C}}_l$. From (9), we have

$$\begin{aligned} c_{1,1} + c_{2,2} + \dots + c_{M,M} &= \left| K P_b h_l^{CH} \right|^2 \sum_m g_m^2 \\ &= \lambda_1 + \lambda_2 + \dots + \lambda_M. \end{aligned} \quad (20)$$

Since $\text{rank}\{\tilde{\mathbf{C}}_l\} = 1$, there is only one non-zero eigenvalue (denoted by λ_1). Thus we can obtain

$$\lambda_1 + \lambda_2 + \dots + \lambda_M = \lambda_1 = \left| K P_b h_l^{CH} \right|^2 \sum_m g_m^2 \quad (21)$$

$$(\lambda \mathbf{I} - \tilde{\mathbf{C}}_l) \mathbf{u} = |K P_b h_l^{CH}|^2
 \begin{bmatrix} g_1^2 - \lambda & \cdots & g_1 g_M e^{j(\alpha_1 - \alpha_M)} \\ \vdots & \ddots & \vdots \\ g_1 g_M e^{j(\alpha_M - \alpha_1)} & \cdots & g_M^2 - \lambda \end{bmatrix} \cdot \begin{bmatrix} u_1 \\ \vdots \\ u_M \end{bmatrix} = \mathbf{0}. \quad (22)$$

$$\begin{bmatrix} -\sum_{m=1, m \neq 1}^M g_m^2 & g_1 g_2 e^{j(\alpha_1 - \alpha_2)} & \cdots & g_1 g_M e^{j(\alpha_1 - \alpha_M)} \\ g_2 g_1 e^{j(\alpha_2 - \alpha_1)} & -\sum_{m=1, m \neq 2}^M g_m^2 & \cdots & g_2 g_M e^{j(\alpha_2 - \alpha_M)} \\ \vdots & \vdots & \ddots & \vdots \\ g_M g_1 e^{j(\alpha_M - \alpha_1)} & g_M g_2 e^{j(\alpha_M - \alpha_2)} & \cdots & -\sum_{m=1, m \neq M}^M g_m^2 \end{bmatrix} \cdot \begin{bmatrix} u_1 \\ \vdots \\ u_M \end{bmatrix} = \mathbf{0}. \quad (23)$$

APPENDIX B

PROOF OF THE ORTHOGONALITY BETWEEN THE STEERING VECTOR $\mathbf{s}(\phi_l, \theta_l)$ AND THE REFERENCE SUBSPACE \mathbf{B}_R

The eigenvectors of the covariance matrix, $\tilde{\mathbf{C}}_l$, are $\mathbf{u}_1, \mathbf{u}_2, \dots, \mathbf{u}_M$. We can solve the characteristic equation of $(\lambda \mathbf{I} - \tilde{\mathbf{C}}_l) \mathbf{u} = \mathbf{0}$ where \mathbf{I} is the unit matrix by (22). By plugging (21) into (22), we can obtain (23).

Let \mathbf{r}_i ($i = 1, 2, \dots, M$) denote the i -th row of the coefficient matrix in (23). Using linear combinations, the rows for $i = 2, 3, \dots, M$ are updated by

$$\mathbf{r}_i - \frac{g_i}{g_1} e^{j(\alpha_i - \alpha_1)} \cdot \mathbf{r}_1 \rightarrow \mathbf{r}_i. \quad i = 2, 3, \dots, M \quad (24)$$

Then we can obtain

$$\begin{bmatrix} -\sum_{m=1, m \neq 1}^M g_m^2 & g_1 g_2 e^{j(\alpha_1 - \alpha_2)} & \cdots & g_1 g_M e^{j(\alpha_1 - \alpha_M)} \\ \frac{g_2}{g_1} e^{j(\alpha_2 - \alpha_1)} \sum_{m=1}^M g_m^2 & -\sum_{m=1}^M g_m^2 & \cdots & 0 \\ \vdots & \vdots & \ddots & \vdots \\ \frac{g_M}{g_1} e^{j(\alpha_M - \alpha_1)} \sum_{m=1}^M g_m^2 & 0 & \cdots & -\sum_{m=1}^M g_m^2 \end{bmatrix} \cdot \begin{bmatrix} u_1 \\ \vdots \\ u_M \end{bmatrix} = \mathbf{0}. \quad (25)$$

Solving the equation set in (25), we can obtain

$$\begin{cases} u_2 = \frac{g_2}{g_1} e^{j(\alpha_2 - \alpha_1)} u_1, \\ \vdots \\ u_M = \frac{g_M}{g_1} e^{j(\alpha_M - \alpha_1)} u_1. \end{cases} \quad (26)$$

It is found that $\mathbf{u}_1 = [g_1 e^{j\alpha_1} \ g_2 e^{j\alpha_2} \ \cdots \ g_M e^{j\alpha_M}]^T$ is a solution of (26), and it is the antenna array's steering vector $\mathbf{s}(\phi_l, \theta_l)$. In other words, the steering vector is the eigenvector \mathbf{u}_1 of the matrix $\tilde{\mathbf{C}}_l$.

Furthermore, as $\tilde{\mathbf{C}}_l$ is a Hermitian matrix and $\lambda_1 \neq \lambda_m = 0$ ($m = 2, 3, \dots, M$), \mathbf{u}_1 is orthogonal to the other eigenvectors, *i.e.*, $\mathbf{u}_1 \perp \mathbf{u}_m, m = 2, 3, \dots, M$. Since $\mathbf{u}_1 = \mathbf{s}(\phi_l, \theta_l)$, the steering vector $\mathbf{s}(\phi_l, \theta_l)$ is orthogonal to the reference subspace spanned by the eigenvectors of $[\mathbf{u}_2 \ \mathbf{u}_3 \ \cdots \ \mathbf{u}_M]$.

REFERENCES

- [1] Y.-H. Nam *et al.*, "Full-dimension MIMO (FD-MIMO) for next generation cellular technology," *IEEE Commun. Mag.*, vol. 51, no. 6, pp. 172–179, Jun. 2013.
- [2] G. Durgin, *Space-Time Wireless Channels*. Englewood Cliffs, NJ, USA: Prentice-Hall, 2003.
- [3] 3GPP, "Study on 3D-channel model for elevation beamforming and FD-MIMO studies for LTE," 3GPP TSG RAN Plenary, Barcelona, Spain, Study Item Description RP-122034, Dec. 2012.
- [4] G. D. Durgin, V. Kukshya, and T. S. Rappaport, "Wideband measurements of angle and delay dispersion for outdoor and indoor peer-to-peer radio channels at 1920 MHz," *IEEE Trans. Antennas Propag.*, vol. 51, no. 5, pp. 936–944, May 2003.
- [5] P. Stoica and K. Sharman, "Maximum likelihood methods for direction-of-arrival estimation," *IEEE Trans. Acoust. Speech Signal Process.*, vol. 38, no. 7, pp. 1132–1143, Jul. 1990.
- [6] R. O. Schmidt, "Multiple emitter location and signal parameter estimation," *IEEE Trans. Antennas Propag.*, vol. AP-34, no. 3, pp. 276–280, Mar. 1986.
- [7] R. Roy and T. Kailath, "ESPRIT-estimation of signal parameters via rotational invariance techniques," *IEEE Trans. Acoust. Speech Signal Process.*, vol. 37, no. 7, pp. 984–995, Jul. 1989.
- [8] N. Yilmazer, J. Koh, and T. K. Sarkar, "Utilization of a unitary transform for efficient computation in the matrix pencil method to find the direction of arrival," *IEEE Trans. Antennas Propag.*, vol. 54, no. 1, pp. 175–181, Jan. 2006.
- [9] T.-J. Shan, M. Wax, and T. Kailath, "On spatial smoothing for direction-of-arrival estimation of coherent signals," *IEEE Trans. Acoust. Speech Signal Process.*, vol. ASSP-33, no. 4, pp. 806–811, Aug. 1985.
- [10] S.-Y. Kung, C. Lo, and R. Foka, "A Toeplitz approximation approach to coherent source direction finding," in *Proc. IEEE Int. Conf. Acoust. Speech Signal Process.*, Apr. 1986, pp. 193–196.
- [11] M. Haardt and J. Nosske, "Unitary ESPRIT: How to obtain increased estimation accuracy with a reduced computational burden," *IEEE Trans. Acoust. Speech Signal Process.*, vol. 43, no. 5, pp. 1232–1242, May 1995.
- [12] J. Chen, S. Wang, and L. Lin, "2-D DOA estimation by MEMP based on L-shape array," in *Proc. 8th Int. Conf. Signal Process.*, Beijing, China, Nov. 2006.
- [13] Y. Tanabe, Y. Ogawa, and T. Ohgane, "High-resolution estimation of multipath propagation based on the 2D-MUSIC algorithm using time-domain signals," *IEICE Trans. Commun.*, vol. 83, no. 4, pp. 407–415, Mar. 2000.
- [14] C. P. Mathews and M. D. Zoltowski, "Eigenstructure techniques for 2-D angle estimation with uniform circular arrays," *IEEE Trans. Signal Process.*, vol. 42, no. 9, pp. 2395–2407, Sep. 1994.
- [15] M. D. Zoltowski, M. Haardt, and C. P. Mathews, "Closed-form 2-D angle estimation with rectangular arrays in element space or beamspace via unitary ESPRIT," *IEEE Trans. Signal Process.*, vol. 44, no. 2, pp. 316–328, Feb. 1996.
- [16] S. Marcos, A. Marsal, and M. Benidir, "The propagator method for source bearing estimation," *J. Signal Process.*, vol. 42, no. 2, pp. 121–138, 1995.
- [17] N. Tayem and H. M. Kwon, "L-shape 2-dimensional arrival angle estimation with propagator method," *IEEE Trans. Antennas Propag.*, vol. 53, no. 5, pp. 1622–1630, May 2005.
- [18] Y. Wu, G. Liao, and H. C. So, "A fast algorithm for 2-D direction-of-arrival estimation," *J. Signal Process.*, vol. 83, no. 8, pp. 1827–1831, 2003.
- [19] C. Li, G. Liao, S. Zhu, and S. Wu, "An ESPRIT-like algorithm for coherent DOA estimation based on data matrix decomposition in MIMO radar," *Elsevier Signal Process.*, vol. 91, no. 8, pp. 1803–1811, 2011.
- [20] Z. Zheng, G. Li, and Y. Teng, "2D DOA estimator for multiple coherently distributed sources using modified propagator," *J. Circuits Syst. Signal Process.*, vol. 31, no. 1, pp. 255–270, 2012.
- [21] Z. Weng and P. M. Djurić, "A search-free DOA estimation algorithm for coprime arrays," *Elsevier Digit. Signal Process.*, vol. 24, pp. 27–33, 2014.
- [22] F. Liu, J. Wang, C. Sun, and R. Du, "Spatial differencing method for DOA estimation under the coexistence of both uncorrelated and coherent signals," *IEEE Trans. Antennas Propag.*, vol. 60, no. 4, pp. 2052–2062, Apr. 2012.
- [23] N. Xi and L. Liping, "A computationally efficient subspace algorithm for 2-D DOA estimation with L-shaped array," *IEEE Signal Process. Lett.*, vol. 21, no. 8, pp. 971–974, Aug. 2014.
- [24] T.-J. Jung and K. Lee, "Closed-form algorithm for 3-D single-source localization with uniform circular array," *IEEE Antennas Wireless Propag. Lett.*, vol. 13, pp. 1096–1099, Jun. 2014.

- [25] B. H. Fleury, M. Tschudin, R. Heddergott, D. Dahlhaus, and K. I. Pedersen, "Channel parameter estimation in mobile radio environments using the SAGE algorithm," *IEEE J. Sel. Areas Commun.*, vol. 17, no. 3, pp. 434–450, Mar. 1999.
- [26] B. H. Fleury, D. Dahlhaus, R. Heddergott, and M. Tschudin, "Wideband angle of arrival estimation using the SAGE algorithm," in *Proc. IEEE 4th Int. Symp. Spread Spectrum Techn. Appl.*, Sep. 1996, pp. 79–85.
- [27] J. Wang, R. Zhang, W. Duan, S. X. Lu, and L. Cai, "Angular spread measurement and modeling for 3D MIMO in urban macrocellular radio channels," in *Proc. IEEE Int. Conf. Commun. Workshop 5G Technol.*, Sydney, NSW, Australia, Jun. 2014, pp. 20–25.
- [28] Y. Zhang, R. Zhang, S. X. Lu, W. Duan, and L. Cai, "Measurement and modeling of indoor channels in elevation domain for 3D MIMO applications," in *Proc. IEEE Int. Conf. Commun. Workshop Small Cell 5G Netw.*, Sydney, NSW, Australia, Jun. 2014, pp. 659–664.
- [29] R. Zhang, L. Cai, X. Lu, P. Yang, and J. Zhou, "Elevation domain measurement and modeling of UMA uplink channel with UE on different floors," in *Proc. IEEE Int. Conf. Comput. Netw. Commun.*, Anaheim, CA, USA, Feb. 2015, pp. 679–684.



Ruonan Zhang (S'09–M'11) received the B.S. and M.S. degrees from Xi'an Jiaotong University, Xi'an, China, and the Ph.D. degree from the University of Victoria, Victoria, BC, Canada, all in the electrical and electronics engineering, in 2000, 2003, and 2010, respectively. From 2003 to 2006, he was with Motorola Inc. and Freescale Semiconductor Inc., Tianjin, China, working on IC architecture and application system design. He is currently an Associate Professor with the School of Electronics and Information, Northwestern Polytechnical University, Xi'an, China. His research interests include wireless channel measurement and modeling, architecture and protocol design of wireless networks, cooperative networking, and satellite communications.



Shichao Wang (S'12) received the B.S. and M.S. degrees from the Northwestern Polytechnical University, Xi'an, China, in 2012 and 2015, respectively. His research interests include wireless channel modeling, communications signal processing, and massive MIMO communications.



Xiaofeng (Stan) Lu received the B.Sc., M.Sc., and Ph.D. degrees in electrical and electronics engineering from Xi'an Jiaotong University, Xi'an, China. He is currently an Algorithm Engineer with Huawei company. His research interests include digital wireless communications, wireless channel measurement and modeling, distributed space-time coding, cooperative communications, and multiple-input multiple-output (MIMO) systems.



Weiming Duan received the M.Sc. degree from the University of Electronic Science and Technology of China, in 1999, and joined Huawei in the same year. His research interests include WCDMA chipset algorithm design, WCDMA UE positioning, LTE system performance evaluation, advanced receiver research, and the 5G air-interface research.



Lin Cai (S'00–M'06–SM'10) received the M.A.Sc. and Ph.D. degrees in electrical and computer engineering from the University of Waterloo, ON, Waterloo, Canada, in 2002 and 2005, respectively. Since 2005, she has been with the Department of Electrical and Computer Engineering, University of Victoria, Victoria, BC, Canada, and she is currently a Professor. Her research interests include span several areas in communications and networking, with a focus on network protocol and architecture design supporting emerging multimedia traffic over wireless, mobile, ad hoc, and sensor networks. She has served as a TPC symposium Co-Chair for IEEE Globecom'10 and Globecom'13 and as the Associate Editor for the IEEE TRANSACTIONS ON WIRELESS COMMUNICATIONS, the IEEE TRANSACTIONS ON VEHICULAR TECHNOLOGY, *EURASIP Journal on Wireless Communications and Networking*, *International Journal of Sensor Networks*, and *Journal of Communications and Networks* (JCN). She was a recipient of the NSERC Discovery Accelerator Supplement Grant in 2010, and the best paper awards of IEEE ICC 2008 and IEEE WCNC 2011.